On the Integration of Subthreshold Inputs from Perforant Path and Schaffer Collaterals in Hippocampal CA1 Pyramidal Neurons

MICHELE MIGLIORE

Section of Neurobiology, Yale University School of Medicine, New Haven, CT, USA; Institute of Biophysics, Nat. Res. Council, Palermo, Italy

migliore@spine.med.yale.edu

Action Editor: E. Bard Ermentrout

Abstract. Using a realistic model of a CA1 hippocampal pyramidal neuron, we make experimentally testable predictions on the roles of the non-specific cation current, I_h, and the A-type Potassium current, I_A, in modulating the temporal window for the integration of the two main excitatory afferent pathways of a CA1 neuron, the Schaffer Collaterals and the Perforant Path. The model shows that the experimentally observed increase in the dendritic density of I_h and I_A could have a major role in constraining the temporal integration window for these inputs, in such a way that a somatic action potential (AP) is elicited only when they are activated with a relative latency consistent with the anatomical arrangement of the hippocampal circuitry.
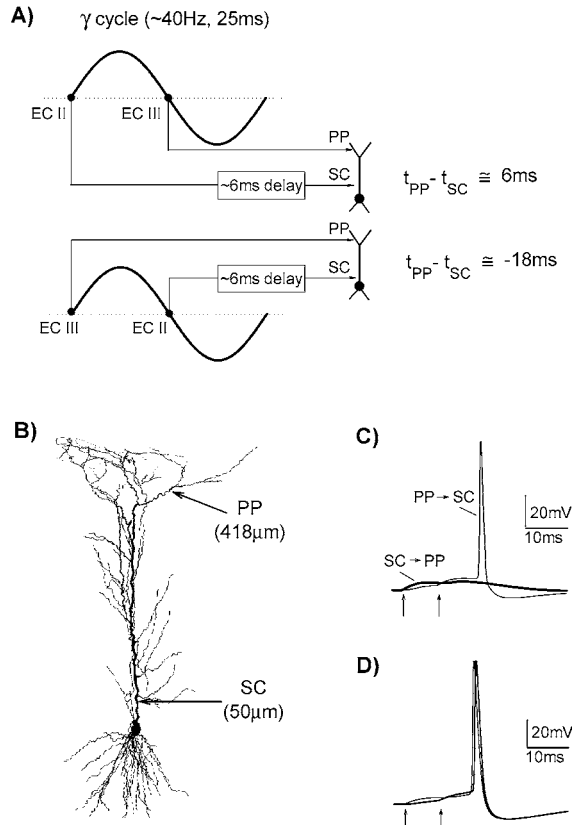
Introduction

Although important details on how dendrites and their active properties are involved in neural computation have been elucidated, the rules according to which dendritic trees and, especially, ionic conductances are developed are still not clear (Migliore and Shepherd, 2002). It has been experimentally shown that dendrites improve the coincidence detection properties of auditory neurons (Agmon-Snir et al., 1998), and experimental findings in CA3 pyramidal neurons (Urban and Barrionuevo, 1998) suggested that a fast 4-AP sensitive K^+ conductance (g_{KA}) might affect the integration of subthreshold inputs. In CA1, the g_{KA} conductance has a major role in modulating the backpropagation of action potentials (APs) (Hoffmann et al., 1997; Migliore et al., 1999), and the non-specific g_h conductance affects the temporal summation window of subthreshold inputs (Magee, 1998, 1999). There are significant differences in the density and dendritic distribution of these two conductances between pyramidal neurons of hippocampus and neocortex. The g_{KA} increases with distance from the soma in CA1, whereas in neocortical neurons it is constant (Korngreen and Sakmann, 2000; Bekkers, 2000), and it does not seem to play the same role as in CA1 (Stuart and Häusser, 2001). The g_h increases in both cases, but it is much higher in neocortical neurons (Williams and Stuart, 1998; Berger et al., 2001). We hypothesize that these differences may reflect different computational roles, and our main aim in this work was to show how and to what extent the integration of subthreshold inputs from the two main excitatory afferent pathways in CA1 could be affected by these conductances. This is particularly important in these neurons, since they fire (on average) at a low rate (Csicsvari et al., 1999). Each AP may thus carry a significant amount of information, and it is then important to elucidate the detailed role of the mechanisms involved in the integration of synaptic inputs that may lead to an AP. We will show, in a realistic model, why

the specific distribution of the g_{KA} and g_h provide CA1 neurons with the ability to integrate their main excitatory synaptic inputs in a way which is especially suited for the anatomical arrangement of the hippocampal circuitry.

Methods

All the simulations were carried out with the NEURON simulation program (Hines and Carnevale, 1997) using its variable time step feature. The realistic model of a hippocampal CA1 pyramidal neuron (Fig. 1B) was that used in a previous work (Migliore et al., 1999),

including a sodium, DR- and A-type potassium currents (I_{Na}, I_{KDR}, and I_A, respectively). A non-inactivating, non-specific cation current $I_h = \bar{g}_h \cdot n \cdot (V - E_{rev})$ was also inserted in the soma and the apical dendrites, with $\bar{g}_h = 1$ pS/μm^2 at the soma. Its activation kinetic was based on the available experimental data for CA1 neurons (Magee, 1998). Thus, the voltage dependence of the activation gate variable was modeled as $n = 1/(1 + \exp(0.151(V - V_{1/2})))$, with $V_{1/2} = -82$ mV in the soma and proximal dendrites (<100 μm), $V_{1/2} = -90$ mV for locations >100 μm from the soma and $E_{rev} = -30$ mV; its time constant was approximated as $\tau_n = \exp(0.033(V - V_t))/(0.011(1 + \exp(0.083(V - V_t))))$, with $V_t = -75$ mV.

Channels Distribution

In CA1 pyramidal neurons, the dendritic densities of I_h and I_A have been directly measured up to $\sim$350 μm in the main trunk of the apical tree (Hoffman et al., 1997; Magee, 1998). There are no quantitative estimations of channels densities in the most distal dendrites or for the smaller oblique branches. However, preliminary observations in CA1 using Calcium imaging (Frick et al., 2002), suggested that the I_A in the proximal oblique dendrites might be higher than in the main trunk at the branch point and, for I_h, an approximately sigmoid increase been shown in neocortical neurons up to $\sim$800 μm (Berger et al., 2001). In the present work, for I_{Na}, I_{KDR}, and I_A, we used the same kinetics and distributions discussed in a previous paper (Migliore et al., 1999). Briefly, as a general rule of thumb we have chosen to use experimental suggestions to implement an effective representation of the real distributions. In particular, the I_{Na} and I_{KDR} were uniformly distributed. The peak conductance for I_A was linearly increased with distance from the soma, d (μm), as $48 \cdot (1 + d/100)$ (pS/μm^2), with dendritic compartments >100 μm from soma having a shifted (-10 mV) activation curve, with respect to more proximal and somatic ones (Hoffman et al., 1997). The peak conductance for I_h was linearly increased as $\bar{g}_h \cdot (1 + 3d/100)$ (Magee, 1998), and all compartments beyond 500 μm from soma or with a diameter smaller than 0.5 μm were considered passive. This choice resulted in good agreement between experiments and modeling results on the role of I_A (Migliore et al., 1999). For simulations using non-uniform passive parameters, R_i (in $\Omega \cdot$ cm) and R_m (in $\Omega \cdot$ cm^2) were increased and decreased,

Figure 1. **A:** Estimation of the boundaries of a physiological time window for the relative activation time ($t_{PP} - t_{SC}$) of PP and SC. **B:** The model neuron and the synaptic locations used in the simulations, SC (50 μm from the soma) and PP (418 μm). **C:** Somatic membrane potential from two simulations. In both cases, the synapses ($\bar{g}_{SC} = 2$ nS, $\bar{g}_{PP} = 12$ nS) were activated with a 8 ms delay, at the time instants indicated by the arrows below the traces. (*light line*, PP $\rightarrow$ SC): the distal synapse (PP) was activated before the proximal one. (*heavy line*, SC $\rightarrow$ PP): the proximal synapse (SC) was activated before the distal one. **D:** As in (C), but with $\bar{g}_{KA}$ reduced by 80%.

respectively, as $R_i = 150 + 300 \cdot d/(300 + d)$ and $R_m = 28000 - 22400 \cdot d/(300 + d)$. Thus, in the distal region ($\sim$400 μm, in our case) R_i was $\sim$2 times higher and R_m $\sim$2 times lower than their values at the soma. About the same change was estimated for R_m in neocortical neurons at the same distance from soma (Stuart and Spruston, 1998).

Synaptic Inputs

In the well-known anatomical arrangement of the hippocampal circuitry (Johnston and Amaral, 1998), the two main excitatory afferent pathways on CA1 neurons, the Perforant Path and the Schaffer Collaterals, originate from neurons of layer II and III of the Entorhinal Cortex that discharge in phase with local gamma oscillations (Chrobak and Buzsáki, 1998). In order to represent them, two excitatory synaptic conductances, g_{SC} and g_{PP}, were modeled using α-functions, with a time constant of 3 ms and reversal potential of 0 mV. They were inserted directly on two dendritic compartments at $\sim$50 and $\sim$420 μm from the soma, respectively, as schematically shown in Fig. 1B. It should be stressed that these conductances model the synchronous activation of a population of synapses, and we assumed the simplest case in which they are activated only once during any given gamma cycle. Several values for the peak synaptic conductance, $\bar{g}_{PP}$ and $\bar{g}_{SC}$ were tested. Only values that were subthreshold for each pathway were used. The NEURON model and simulation files are publicly available under the ModelDB section of the Senselab database (http://senselab.yale.med.edu).

Results

In vivo, the Perforant Path fibers from layer III of the Entorhinal Cortex (ECIII) contact the distal apical tree of a CA1 pyramidal neuron, whereas the input from EC layer II (ECII) is elaborated by the Dentate Gyrus and CA3 networks before contacting the proximal apical tree as Schaffer Collaterals. Although the relative strength, location, and activation time of these pathways may depend on a number of factors, their basic arrangement is maintained across different mammalian species.

The ECII-III neurons firing in phase with local γ oscillations, which have an important role in both perceptual binding and attention (Gray et al., 1989; Fries et al., 2001), suggests that they most likely carry information on related items/events that need to be elaborated by the hippocampus within an appropriate (physiological) time window related to the γ cycle. Thus, in order to investigate the effects of the dendritic properties on the synaptic integration of the two inputs, we first estimated the boundaries of this window as schematically shown in Fig. 1A. The limit cases are when the two inputs are activated with an 180° phase difference during the positive sweep of the same γ cycle. Assuming for the ECII input an additional 6 ms of synaptic conduction delay, to propagate within the hippocampal circuitry, the relative activation times on CA1 ($t_{PP} - t_{SC}$) could be anywhere from about −18 ms (Fig. 1A, bottom) to +6 ms (Fig. 1A, top), with an increasing probability toward the peak of the cycle. Of course, this is an approximate estimation and we thus used a fading gray area to schematically indicate a physiological time window. It should be stressed, however, that our estimate is consistent with what has been experimentally found in rabbits, where the two pathways were activated in vivo with a relative delay of $\sim$3–15 ms, with the Perforant Path input preceding the Schaffer Collaterals (Yeckel and Berger, 1998).

The physiological arrangement of these pathways in vivo should result in an asymmetry in the temporal window for the "coincidence detection" of the two inputs, depending on their relative electrotonic distance (Rall, 1964; for a review of dendritic integration see also Spruston et al., 1999). In fact, the physiological arrangement was reproduced in the simulations of Fig. 1C, where SC and PP were activated with the same delay but in a different order. As can be seen, only when PP was activated before SC (Fig. 1C, light line, PP → SC) an AP was elicited at the soma, and not vice versa (Fig. 1C, heavy line, SC → PP). At first, it could be considered as trivial that the more distal input must be initiated first before it can be effectively summated with a proximal one at the soma, since it must travel farther. Our model suggests that this is not the case in CA1 neurons, as illustrated by the simulations in Fig. 1D, where $\bar{g}_{KA}$ was reduced by 80% and the synaptic conductances were adjusted to give the same peak somatic depolarization as in Fig. 1C. In this case, an AP was elicited independently from the activation order of the two inputs, in agreement with the experimental findings in CA3 pyramidal neurons, showing that a 4-AP sensitive K$^+$ current could be involved with this effect (Urban and Barrionuevo, 1998).

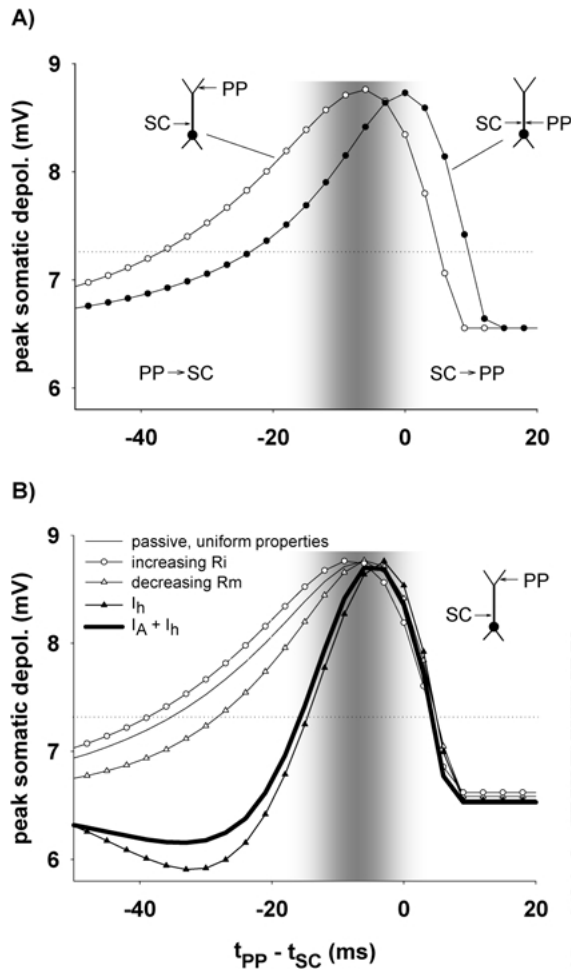The results of Fig. 1D showed a direct role for I_A. However, other passive or active properties may

A)

B)

Figure 2. **A:** Peak somatic depolarization vs relative activation time in a passive model with uniform properties and synaptic inputs in different dendritic regions. **B:** Peak somatic depolarization in a passive model with non-uniform properties or with I_h and I_{KA}.

Table 1. Peak conductances, $\bar{g}_{SC}$ and $\bar{g}_{PP}$, to obtain the same somatic depolarization ($\sim$6.5 and $\sim$2.5 mV, respectively) in the simulations for Fig. 2.

(nS)	Passive			Active	
	Uniform	Increasing (R_i)	Decreasing (R_m)	I_h	$I_h + I_{KA}$
$\bar{g}_{SC}$, 50 μm	2.25	2.05	2.3	2.35	2.85
$\bar{g}_{PP}$, 418 μm (50 μm)	1.65 (0.85)	2.0	1.9	2.55	20.0

modulate the temporal window, especially those affecting the temporal summation of synaptic inputs. In order to assess the relative contribution of the mechanisms involved, we then investigated the different roles that may be played by the passive dendritic tree, the I_h, and the I_A. The results are illustrated in Fig. 2, where we plot the peak somatic depolarization as a function of the relative activation times under different conditions. In order to compare the results, in all cases no sodium channels were used, and the synaptic strengths (reported in Table 1) were adjusted to obtain the same somatic depolarization for SC and PP ($\sim$6.5 mV and $\sim$2 mV, respectively, in this case) when they were independently activated. The AP threshold of the full model is indicated by a dotted line, and the part of the curves above

this line thus indicates when an AP would be elicited. Let's consider first the case in which the two inputs targeted the same dendritic location (Fig. 2A, closed symbols). In the trivial case in which they also have the same strength (data not shown), the peak somatic depolarization was a bell-shaped curve centered at 0 ms. However, when we used different relative strengths the results depended on their activation order, as shown in Fig. 2A for the SC > PP case. In particular, a more favorable condition, with respect to the physiological time window, was obtained when the weaker input preceded the stronger one (Fig. 2A, $t_{PP} - t_{SC} < 0$ ms). However, it would not be possible to distinguish between activation of PP $\rightarrow$ SC with SC > PP (as in Fig. 2A) or SC $\rightarrow$ PP with SC < PP, since they will give identical results when SC and PP target the same region. The important information on the specific activation order would thus be lost. One (partial) solution to this problem is to develop a dendritic tree, and direct the PP input (which in vivo is most likely activated before SC) to an electrotonically more distant location. As shown in Fig. 2 (open symbols), this has two important effects: (a) PP will most likely be the weaker pathway at the soma, because of the attenuation due to the passive flow; (b) it introduces a temporal asymmetry in the integration of the two inputs, shifting the relative activation time for the maximum somatic depolarization within the physiological time window.

A distal dendritic location for PP, however, is still not sufficient to fulfill the kind of information processing in which CA1 neurons and their afferents are supposedly involved (Treves and Rolls, 1994). The time window for which an AP would be elicited is still too large, with respect to the physiological time window (Fig. 2A, open symbols for $t_{PP} - t_{SC} < -20$ ms). Since recent experimental findings in neocortical pyramidal neurons (Stuart and Spruston, 1998) suggested that the dendritic passive properties might not be uniform throughout the cell, it could be argued that a non-uniform distribution

of R_m or R_i may help in reducing the time window, because they affect the membrane time constant and the electrotonic length of the neuron. In the typical examples shown in Fig. 2B for R_m and R_i, we show the amount of change that could be expected in these cases. As can be seen (Fig. 2B, open triangles) decreasing R_m somewhat reduced the time window, thus improving the correct detection of the two inputs, whereas the opposite result was obtained increasing R_i. Much better results were however obtained when the I_h and I_A were included in the model with uniform passive parameters (Fig.2B, closed triangles and thick line). The I_h, in particular, occluded the effects on the time window caused by I_A alone (data not shown).

It may thus appear that a combination of non-uniform passive properties and I_h could ensure that subthreshold PP and SC inputs would be detected only when they are activated within the appropriate time window. However, the model indicated another potential problem. As stated before, to compare the effects of different properties on the time window, $\bar{g}_{PP}$ and $\bar{g}_{SC}$ were independently adjusted to give approximately the same depolarization at the soma. As shown in Table 1, in almost all cases their values were of the same order of magnitude. This implies that a distal PP input could easily be of suprathreshold strength, eliciting an AP even in the absence of any SC input. A dendritic I_A, with its "shock absorber" function (Yuste, 1997), would require a much stronger distal input even for a relatively low somatic depolarization (see the $\bar{g}_{PP}$ value for $I_h + I_A$ in Table 1), making extremely difficult for a PP input to elicit a somatic AP.

We next studied the effects of the dendritic g_{KA}. It has been experimentally shown that the g_{KA} conductance in CA1 neurons has peculiar characteristics (Hoffman et al., 1997). In contrast with what was found, for example, in pyramidal neocortical neurons (Korngreen and Sakmann, 2000; Bekkers, 2000), its density increases with the distance from the soma, and the kinetic of activation in the distal ($>100\ \mu$m) dendrites is shifted (-10 mV) with respect to that at the soma. We thus investigated the effects of a different kinetic and distribution of dendritic I_A, and the results are shown in Fig. 3. In the full model, all APs were elicited within the physiological time window for a wide range of $\bar{g}_{PP}$ values (Fig. 3, closed symbols). The range of subthreshold $\bar{g}_{PP}$ values was drastically limited using a uniform distribution of dendritic $\bar{g}_{KA}$ (at somatic density), as in neocortical neurons (Fig. 3, open circles). The useful range of $\bar{g}_{PP}$ was also reduced using a $+10$ mV
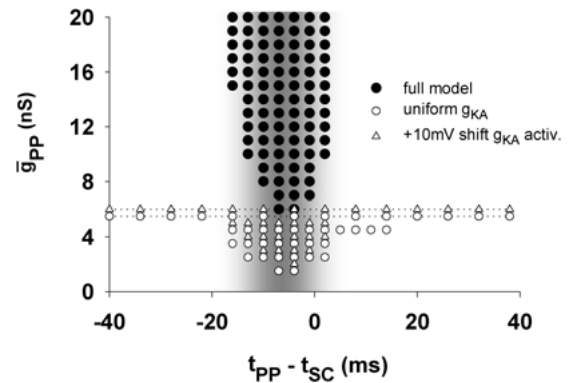

Figure 3. APs generated by activation of SC and PP for a given combination of relative activation times ($t_{PP} - t_{SC}$) and peak PP conductance, $\bar{g}_{PP}$ using a full model (*closed symbols*), a uniform g_{KA} (*open circles*), or a $+10$ mV shift in the activation curve of the dendritic ($>100\ \mu$m) g_{KA} (*triangles*). Dotted lines mark suprathreshold values of $\bar{g}_{PP}$. In all cases $\bar{g}_{SC} = 3.5$ nS.

shift in the dendritic ($>100\ \mu$m) g_{KA} activation curve (Fig. 3, triangles), to model activity-dependent modulations (reviewed in Johnston et al., 2000) that result in the dendritic channel kinetics being similar to the somatic ones. These findings suggest that the different kinetic and distribution of the dendritic g_{KA}, with respect to other pyramidal neurons, may reflect a need for a specific modulation of synaptic integration (Migliore and Shepherd, 2002).

The role of g_h in the dendritic integration of the PP and SC inputs in CA1 neurons is illustrated by the simulations in Fig. 4, where we show simulations findings for different combinations of g_h and g_{KA} distributions. With respect to the full model (Fig. 4, closed circles), a uniform dendritic distribution (at somatic density) of g_h, did not result in major differences (Fig. 4, open circles). However, a uniform dendritic distribution of g_h, in addition to any change reducing the effects of the dendritic g_{KA}, such as a uniform distribution (Fig. 4, closed triangles) a reduced density (as in Fig. 1D) or a $+10$ mV shift in its activation (data not shown), resulted in APs elicited for a wide range of relative activation times, and well outside the physiological time window. Instead, a uniform g_{KA} with a normal (i.e. increasing with distance) g_h (Fig. 4, open triangles) resulted in APs elicited within the physiological time window, although for a limited range of PP. These results suggest that, in CA1 neurons, an increasing density of dendritic g_h could be needed to maintain the temporal integration window of SC and PP inputs within its physiological limits when the effects of the g_{KA} channels are reduced
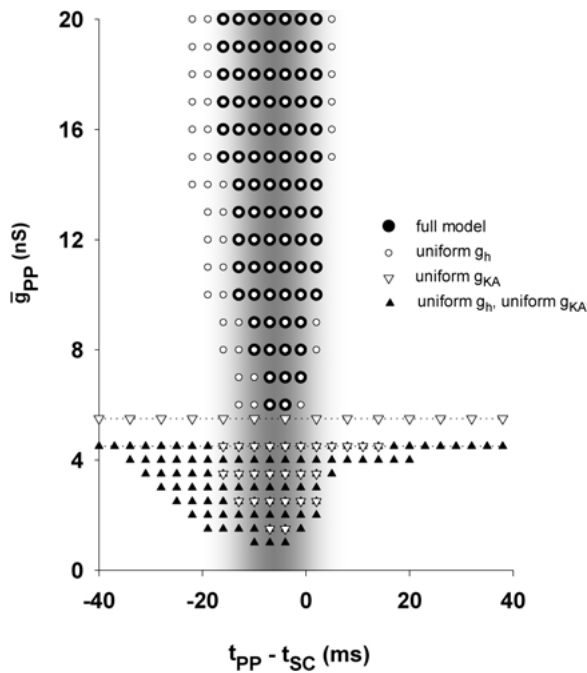
Figure 4. APs generated by activation of SC and PP for a given combination of relative activation times ($t_{PP} - t_{SC}$) and peak PP conductance, $\bar{g}_{PP}$, using different distributions of g_{KA} and g_h: full model (*closed circles*), uniform distribution of g_h (*open circles*), uniform distribution of g_{KA} (*open triangles*), uniform distribution of g_{KA} and g_h (*close triangles*). Dotted lines mark suprathreshold values of $\bar{g}_{PP}$. In all cases $\bar{g}_{SC} = 3.5$ nS.

because of dendritic depolarization (that inactivates the g_{KA}) or protein kinases activation (that shifts the activation curve).

The reasons why the I_A and I_h resulted in the observed effects are directly related to their experimentally known properties of signal attenuation (Hoffman et al., 1997) and normalization of the EPSPs time course (Williams and Stuart, 2000), respectively. These features are reproduced by our model, and their effects on the temporal summation of PP and SC are illustrated by the typical examples shown in Fig. 5, were we report simultaneous somatic and dendritic membrane potential for $t_{PP} - t_{SC} = -20$ ms, $\bar{g}_{SC} = 3.5$ nS, and $\bar{g}_{PP} = 4$ nS. Under these conditions, an AP was not elicited in the full model (Fig. 5, heavy lines), mainly because the strong attenuation, exerted by the g_{KA} on any dendritic depolarization from the resting potential, prevented an effective summation of the two inputs. A uniform dendritic distribution of g_{KA} reduced its effects, resulting in an overall amplification of the distal PP input that, however, when summated with SC, was
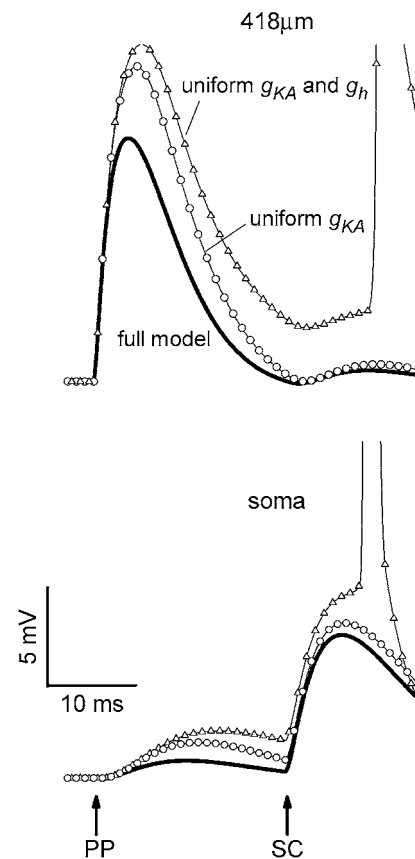

Figure 5. Dendritic (top panel, 418 μm) and somatic (bottom panel) membrane potential from simulations in which the synapses ($\bar{g}_{SC} = 3.5$ nS, $\bar{g}_{PP} = 4$ nS) were activated with a 20 ms delay, with PP preceding SC, using different dendritic distributions of g_{KA} and g_h: full model (*heavy lines*), uniform distribution of g_{KA} (*circles*), uniform distribution of g_{KA} and g_h (*triangles*).

still not sufficient to elicit a somatic AP (Fig. 5, circles), because of the effects of g_h on the temporal summation of synaptic inputs (Magee, 1998, 1999; Williams and Stuart, 2000; Berger et al., 2001). In fact, the g_h curtailed the distal PP input and an AP was elicited only when a uniform dendritic distribution of g_h was also used (Fig. 5, compare triangles and circles).

The Shaffer Collateral and the Perforant Path inputs may target a large extent of the CA1 apical tree within the stratum radiatum and stratum lacunosum-moleculare, respectively. Thus, several locations for the SC (0–250 μm) and PP (250–500 μm) inputs were investigated, in order to test how and to what extent the temporal integration window could be affected. As discussed before, the best case is when the two pathways are relatively distant, whereas the worst case is when
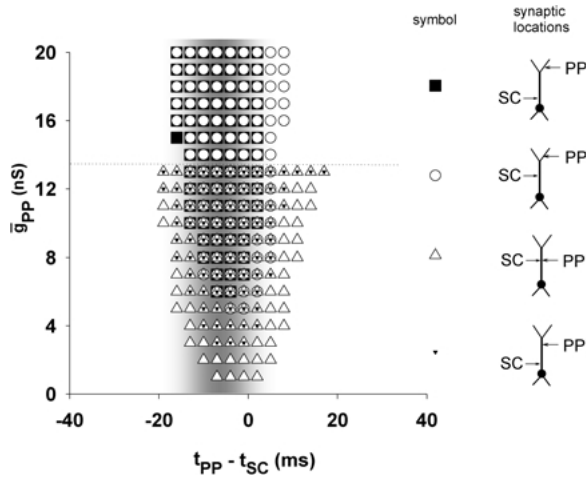
Figure 6. APs generated by activation of SC and PP for a given combination of relative activation times ($t_{PP} - t_{SC}$) and peak PP conductance, $\bar{g}_{PP}$, with a full model using different synaptic locations for SC and PP: (*closed squares*) 50 and 420 μm, (*open circles*) 200 and 420 μm, (*open triangles*) 250 and 250 μm, (*closed triangles*) 50 and 300 μm, respectively. In all cases $\bar{g}_{SC}$ was adjusted in such a way to obtain the same peak somatic depolarization when activated alone. The dotted line marks suprathreshold values of $\bar{g}_{PP}$ for the open and closed triangles cases.

they target the same dendritic location. The simulation findings for a few typical relative locations are shown in Fig. 6. In all cases, most APs were elicited within the physiological time window for a wide range of PP values, including the (computationally) worst case in which PP and SC targeted the same location (250 μm, Fig. 6, open triangles).

Discussion

Our findings suggest that the specific densities and distribution of dendritic g_{KA} and g_h in CA1 neurons may reflect specific computational requirements for temporal integration of the Perforant Path and Schaffer Collateral inputs. Although more elaborated input pathways (in terms of subcellular anatomy, function, composition, modulation, type of information carried, etc) were not taken into account in this paper, several basic, experimentally testable, predictions may be drawn from our model. First, although the densities and distribution of g_{KA} and g_h, as observed in these neurons, result in a temporal integration window for the SC and PP inputs that is robust for different synaptic locations, a relatively distant location is needed to avoid that the two pathways become indistinguishable. If they target

the same location, a CA1 neuron could elicit an AP integrating, in the wrong order, an input from ECIII with an input originating several ms earlier in ECII that may refer to an unrelated item. Furthermore, the g_h will reduce the temporal window into the appropriate range, but will not prevent a strong PP input, unprocessed by the hippocampal network, to elicit a somatic AP. The high density and shifted kinetics of dendritic g_{KA} are then needed for a strong (and non-linear) attenuation of a distal input during its somatopetal propagation. This, finally, ensures that a somatic AP will be preferentially elicited following a *Perforant Path → Schaffer Collateral* activation within the appropriate time window and for a wide range of $\bar{g}_{PP}$. It should be stressed that our results are consistent with experimental findings suggesting that, in CA1, the distal excitatory synapses could be much stronger than the proximal ones (Magee and Cook, 2000; Megías et al., 2001).

All the model predictions are experimentally testable. Surprisingly, even the basic effect of the temporal asymmetry in the detection of two subthreshold SC and PP inputs, has never been experimentally investigated in CA1. It can be experimentally tested with the available electrophysiological techniques, whereas how I_h and I_A affect the time window and the range of PP inputs could be experimentally tested by the standard pharmacological manipulations used to block these currents.

More generally, our findings give a deeper insight on how the active and morphological properties of the dendritic tree may be developmentally adapted to fit the computational role of a neuron. They directly point out that one of the rules according to which dendritic trees and active properties might be developed is to detect temporal differences and control the range of synaptic inputs that could elicit an AP. The presence of long primary dendrites, such as in the hippocampal CA1 or deep neocortical neurons, that favor location-dependent somatic depolarization by synaptic inputs (Jaffe and Carnevale, 1999), could indicate a need for a specific, asymmetric, temporal integration window. According to our model, the different distributions of g_{KA} and g_h in different neurons may suggest how distal inputs should be elaborated. For CA1, the high-density distribution of g_{KA} may indicate a distal input that should not be able to trigger an output (a somatic AP), unless it is complemented by a further, more proximal, input. An increasing density of g_h may be needed to constrain the temporal integration time window within the physiological limits under those circumstances in

which the effects of the g_{KA} are reduced. For neocortical neurons, instead, a uniform and relatively lower density of g_{KA} may indicate the need for a distal input to be able to independently trigger an output (Larkum et al., 2001), with a higher density of g_h that, by further constraining the temporal window, effectively improves the local independent processing of synaptic inputs (Berger et al., 2001).

Acknowledgments

References

Agmon-Snir H, Carr CE, Rinzel J (1998) The role of dendrites in auditory coincidence detection. Nature 393: 268–272.

Berger T, Larkum ME, Luscher HR (2001) High I(h) channel density in the distal apical dendrite of layer V pyramidal cells increases bidirectional attenuation of EPSPs. J. Neurophysiol. 85: 855–868.

Chrobak JJ, Buzsáki G (1998) Gamma oscillations in the entorhinal cortex of the freely behaving rat. J. Neurosci. 18: 388–398.

Csicsvari J, Hirase H, Czurko A, Mamiya A, Buzsáki G (1999) Oscillatory coupling of hippocampal pyramidal cells and interneurons in the behaving rat. J. Neurosci. 19: 274–287.

Frick A, Magee JC, Johnston D (2001) Ca^{2+} signals from backpropagating action potentials in small oblique dendrites of CA1 pyramidal neurons, Soc. Neurosci. Abs., Vol. 31.

Fries P, Reynolds JH, Rorie AE, Desimone R (2001) Modulation of oscillatory neuronal synchronization by selective visual attention. Science 291: 1560–3563.

Gray CM, Konig P, Engel AK, Singer W (1989) Oscillatory responses in cat visual cortex exhibit inter-columnar synchronization which reflects global stimulus properties. Nature 338: 334–337.

Hines M, Carnevale T (1997) The NEURON simulation environment. Neural Comp. 9: 178–1209.

Hoffman DA, Magee JC, Colbert CM, Johnston D (1997) K$^+$ channel regulation of signal propagation in dendrites of hippocampal pyramidal neurons. Nature 387: 869–875.

Jaffe DB, Carnevale NT (1999) Passive normalization of synaptic integration influenced by dendritic architecture. J. Neurophysiol. 82: 3268–3285.

Johnston D, Amaral DG (1998) Hippocampus. In: GM Shepherd, ed. The Synaptic Organization of the Brain, 4th edn. Oxford Univ. Press, New York, pp. 417–458.

Johnston D, Hoffman DA, Magee JC, Poolos NP, Watanabe S, Colbert CM, Migliore M (2000) Dendritic potassium channels in hippocampal pyramidal neurons. J. Physiol. 525: 75–81.

Korngreen A, Sakmann B (2000) Voltage-gated K$^+$ channels in layer 5 neocortical pyramidal neurones from young rats: Subtypes and gradients. J. Physiol. 525: 621–639.

Larkum ME, Zhu JJ, Sakmann B (2001) Dendritic mechanisms underlying the coupling of the dendritic with the axonal action potential initiation zone of adult rat layer 5 pyramidal neurons. J. Physiol. 533: 447–466.

Magee JC (1998) Dendritic hyperpolarization-activated currents modify the integrative properties of hippocampal CA1 pyramidal neurons. J. Neurosci. 18: 7613–7624.

Magee JC (1999) Dendritic Ih normalizes temporal summation in hippocampal CA1 neurons. Nat Neurosci. 2: 508–514.

Magee JC, Cook E (2000) Somatic EPSP amplitude is independent of synapse location in hippocampal pyramidal neurons. Nature Neurosci. 3: 895–903.

Megías M, Emri ZS, Freund TF, Gulyás AI (2001) Total number and distribution of inhibitory and excitatory synapses on hippocampal CA1 pyramidal cells. Neuroscience 102: 527–540.

Migliore M, Hoffman DA, Magee JC, Johnston D (1999) Role of an A-type K$^+$ conductance in the back-propagation of action potentials in the dendrites of hippocampal pyramidal neurons. J. Comput. Neurosci. 7: 5–16.

Migliore M, Shepherd GM (2002) Emerging rules for the distributions of active dendritic conductances. Nature Rev. Neurosci. 3: 362–370.

Rall W (1964) Theoretical significance of dendritic trees for neuronal input-output relations. In: RF Reiss, ed. Neural Theory and Modeling. Stanford University Press, Palo Alto, CA, pp. 73–97.

Spruston N, Häusser M, Stuart G (1999) Dendritic integration. In: G Stuart, N Spruston, M Häusser, eds. Dendrites. Oxford University Press, New York, NY, pp. 231–260.

Stuart GJ, Häusser M (2001) Dendritic coincidence detection of EPSPs and action potentials. Nature Neurosci. 4: 63–71.

Treves A, Rolls ET (1994) Computational analysis of the role of the hippocampus in memory. Hippocampus 4: 374–391.

Urban NN, Barrionuevo G (1998) Active summation of excitatory postsynaptic potentials in hippocampal CA3 pyramidal neurons. Proc. Natl. Acad. Sci. USA 95: 11450–11455.

Williams SR, Stuart GJ (2000) Site independence of EPSP time course is mediated by dendritic I(h) in neocortical pyramidal neurons. J. Neurophysiol 83: 3177–3182.

Yeckel MF, Berger TW (1998) Spatial distribution of potentiated synapses in hippocampus: Dependence on cellular mechanisms and network properties. J. Neurosci. 18: 438–450.

Yuste R (1997) Potassium channels: Dendritic shock absorbers. Nature 387: 851–853.